

# Influence of ambipolar potential on the properties of inductively coupled discharges at the bounce resonance condition

Oleg V. Polomarov and Constantine E. Theodosiou

*Department of Physics and Astronomy, University of Toledo, Toledo, Ohio, 43606-3390.*

Igor D. Kaganovich

*Plasma Physics Laboratory, Princeton University, Princeton, NJ 08543*

(Dated: March 15, 2018)

The importance of accounting for an ambipolar electrostatic potential or a non-uniform density profile for modelling of inductively coupled discharges is demonstrated. A drastic enhancement is observed of the power transfer into plasma for low-collisional, low-pressure, non-local discharges with non-uniform electron density profiles under the condition of bounce resonance. This enhanced plasma heating is attributed to the increase of the number of resonant electrons, for which the bounce frequency inside the potential well is equal to the rf field frequency.

## INTRODUCTION

Low pressure radio-frequency (rf) inductive discharges have been extensively used over the past decade as sources of inductively coupled plasmas (ICP) in the plasma aided material processing industry, semiconductor manufacturing, and lighting [1, 2]. For very low pressures, i.e. in the milli-Torr region the ICP discharges exhibit a strong non-local behavior and a number of peculiar physical effects typical for warm plasmas, like an anomalous skin penetration and a resonant wave-particle interaction [3, 4]. The study of these effects leads to further optimization of the ICP sources and can result in improvement of the characteristics of plasma-based devices.

An interesting effect that can lead to enhanced heating for bounded, low-pressure plasmas is the possible bounce resonance between the frequency  $\omega$  of the driving rf field and the frequency of the bounce motion of the plasma electrons confined in the potential well by an ambipolar potential  $\phi(x)$  and the sheath electric fields near the discharge walls [5, 6, 7, 8, 9, 10, 11]. Most earlier theoretical and numerical studies on this subject assumed for simplicity a uniform plasma density over the discharge length, and the absence of an ambipolar potential, i.e. allowed the electrons to bounce inside a potential that is flat inside the plasma and infinite at the walls [8, 10, 11, 12, 13]. Although these suppositions can result in a fairly good description of the plasma behavior under non-resonant conditions, the discharge parameters under resonant conditions can be greatly altered by accounting for the presence of the ambipolar potential, which – it should be stressed – always exists in real discharges. It is a very well known result of the quasilinear theory, that for low-collisional discharges the plasma heating essentially depends on the so-called “resonant electrons,” or electrons with velocities equal to the phase velocities  $v \simeq \omega/k$  of the plane waves constituting the rf field (Landau damping) [6, 7]. For bounded plasmas and for an

electron to be resonant, the above condition transforms into the requirement that the rf field frequency must be equal to, or be an integer multiple of the bounce electron frequency  $\omega = n\Omega_b$ . But the electron bounce frequency is very sensitive to the actual shape of the ambipolar electrostatic potential  $\phi(x)$ , especially for low-energy electrons. Accounting for the electrostatic potential can lead the plasma electrons into the resonant region even if they were not there in the absence of the potential. This can result into a drastic enhancement of the plasma heating and other related phenomena [14].

In this article we present the results of a full, self-consistent numerical modelling of low pressure ICP discharges under the bounce resonance condition and show the pronounced influence of the presence of the electrostatic ambipolar potential on the plasma parameters under resonant conditions.

## BASIC EQUATIONS

The model assumes a one-dimensional, slab geometry, inductively coupled discharge of a plasma bounded on both sides by parallel walls with a gap length  $L$ . The walls carry fixed currents flowing in opposite directions, produced by an external radio frequency source. The induced solenoidal rf electric field  $E_y$  is directed along the walls and the static ambipolar electric field  $E_x = -d\phi/dx$  of the ambipolar potential  $\phi(x)$  is directed towards the discharge walls, keeping electrons confined and the plasma quasineutral, i.e.  $n_e(x) = n_i(x)$ . In the present treatment of high density discharge plasmas ( $n_e \sim 10^8 - 10^{12} \text{ cm}^{-3}$ ) the sheath width is neglected, because it is of the order of a few hundreds of microns, much less than the discharge dimension  $L$ . Furthermore, it is assumed that the plasma electrons experience specular reflection: a) from the discharge walls when they have total energy  $\varepsilon = mv^2/2 - e\phi(x)$  larger than the electron potential energy  $-e\phi(x_w)$  at the walls,  $\pm x_w$ , and b) from the geometrical location of the turning points

$x_{\pm}(\varepsilon)$ , where  $-e\phi(x_{\pm}) = \varepsilon$ . The above 1-D scheme can also be a good approximation for a cylindrical ICP discharge, if the rf field penetration depth  $\delta$  into the plasma is less than the plasma cylinder radius  $R$  [16].

In order to describe the discharge self-consistently, one needs to determine the rf electric field profile  $E_y(x)$ , the electron energy distribution function (EEDF)  $f_0(\varepsilon)$ , and the ambipolar potential  $\phi(x)$ . The detailed description of all the needed formalism is given in [15]. A short account of the formalism is given below.

### Calculation of the EEDF

For low-pressure discharges, where the energy relaxation length is large compared with the plasma width and the energy relaxation time is large compared with the rf period, the electron velocity distribution function (EVDF) can be represented as a sum of the main isotropic part  $f = f_0(\varepsilon)$  (EEDF) that is a function of only the total energy  $\varepsilon$  and of a small alternating anisotropic part  $f_1(x, \mathbf{v}, t)$ ,  $f = f_0(\varepsilon) + f_1(x, \mathbf{v}, t)$  [17, 18, 19]. The Boltzmann equation for the electron velocity distribution function reads

$$\frac{\partial f_1}{\partial t} + v_x \frac{\partial f_1}{\partial x} + \frac{e}{m} \frac{d\phi}{dx} \frac{\partial f_1}{\partial v_x} - \frac{eE_y(x, t)}{m} \frac{\partial (f_0 + f_1)}{\partial v_y} = St(f_1 + f_0), \quad (1)$$

where  $E_y(x, t)$  is the nonstationary rf electric field, and  $St(f)$  is the collision integral. After applying the standard quasilinear theory, Eq.(1) splits into two equations [6], a linear one for  $f_1$

$$\frac{\partial f_1}{\partial t} + v_x \frac{\partial f_1}{\partial x} + \frac{e}{m} \frac{d\phi}{dx} \frac{\partial f_1}{\partial v_x} - \frac{eE_y(x, t)}{m} \frac{\partial f_0}{\partial v_y} = St(f_1), \quad (2)$$

and a quasilinear one for  $f_0$

$$-\overline{\frac{eE_y(x, t)}{m} \frac{df_1}{dv_y}} = \overline{St(f_0)}. \quad (3)$$

Here, the bar denotes space-time averaging over the phase space available to electrons with total energy  $\varepsilon$  [17, 18, 19]. We can represent as harmonic functions the rf electric field  $E_y(x, t) = E_{y0}(x) \exp(-i\omega t)$  and the anisotropic part of the EVDF  $f_1 = f_{10} \exp(-i\omega t)$ , where  $\omega$  is the discharge frequency. Using the Bhatnagar-Gross-Krook (BGK) approximation [15],  $St(f_1) = -\nu f_1$ , and omitting the subscript 0 in the amplitudes, Eq. (2) can be rewritten as

$$-i\omega f_1 + v_x \frac{\partial f_1}{\partial x} \Big|_{\varepsilon_x} - ev_y E_y(x) \frac{df_0}{d\varepsilon} = -\nu f_1, \quad (4)$$

where  $\nu$  is the transport collision frequency,  $\varepsilon_x = mv_x^2/2 + \varphi(x)$  is the total energy along the  $x$ -axis, and  $\varphi(x) = -e\phi(x)$  is the electron potential energy.

Eq. (4) can be effectively solved using a Fourier series expansion. Introducing the variable angle of the bounce motion [19] which is proportional to the time of flight of an electron from the left turning point to the current point

$$\theta(x, \varepsilon_x) = \frac{\pi \text{sgn}(v_x)}{T(\varepsilon_x)} \int_{x_-}^x \frac{dx}{|v_x(\varepsilon_x)|}, \quad (5)$$

where  $T$  is half of the bounce period of the electron motion in the potential well  $\varphi(x)$

$$T_b(\varepsilon_x) = \int_{x_-}^{x_+} \frac{dx}{|v_x(\varepsilon_x)|}, \quad (6)$$

Eq. (4) simplifies to

$$-i\omega f_1 + \Omega_b \frac{\partial f_1}{\partial \theta} \Big|_{\varepsilon_x} - v_y e E_y(\theta) \frac{df_0}{d\varepsilon} = -\nu f_1. \quad (7)$$

where  $\Omega_b(\varepsilon_x) = \pi/T(\varepsilon_x)$  is the bounce frequency for the electron in the potential well. Making use of the Fourier series

$$g(x, \varepsilon_x) = \sum_{n=-\infty}^{\infty} g_n \exp(in\theta), \quad (8)$$

$$g_n = \frac{1}{2\pi} \left[ \int_{-\pi}^{\pi} g(\theta, \varepsilon_x) \exp(-in\pi\theta) d\theta \right], \quad (9)$$

Eq. (7) gives

$$E_{yn}(\varepsilon_x) = \frac{1}{\pi} \left[ \int_0^{\pi} E_y(\theta) \cos(n\theta) d\theta \right], \quad (10)$$

and

$$\begin{aligned} f_{1s}(x, \varepsilon_x) &\equiv 1/2(f_1(v_x > 0) + f_1(v_x < 0)) \\ &= -mv_y V_y^{\text{rf}}(x, \varepsilon_x) \frac{df_0}{d\varepsilon}, \end{aligned} \quad (11)$$

where

$$V_y^{\text{rf}}(x, \varepsilon_x) = -\frac{e}{m} \sum_{n=-\infty}^{\infty} \frac{E_{yn} \cos[n\theta(x)]}{in\Omega_b - i\omega + \nu}. \quad (12)$$

Knowing the symmetrical part  $f_{1s}$  of the anisotropic contribution to the EVDF, one can average Eq. (3) according to

$$\overline{\text{Term}(x, \mathbf{v})}(\varepsilon) = \int_{x_-}^{x_+} dx v(x, \varepsilon) \text{Term}[x, v(x, \varepsilon)], \quad (13)$$

$$v(x, \varepsilon) = \sqrt{2[\varepsilon - \varphi(x)]/m}. \quad (14)$$

and obtain the final equation for  $f_0$

$$\begin{aligned} -\frac{d}{d\varepsilon} (D_\varepsilon + \overline{D_{ee}}) \frac{df_0}{d\varepsilon} - \frac{d}{d\varepsilon} [\overline{V_{ee}} + \overline{V_{el}}] f_0 = \\ \sum_k \left[ \overline{\nu_k^* (w + \varepsilon_k^*) \frac{\sqrt{(w + \varepsilon_k^*)}}{\sqrt{w}} f_0(\varepsilon + \varepsilon_k^*) - \overline{\nu_k^*} f_0} \right]. \end{aligned} \quad (15)$$

Here, the bar denotes averaging according to Eq. (13), and  $\nu_k^*$  is the inelastic collision frequency. The coefficients  $V_{el}, D_{ee}, V_{ee}$  stem from the elastic and electron-electron collision integrals, respectively, and are given by [18, 21]

$$V_{el} = \frac{2m}{M} w \nu, \quad (16)$$

$$V_{ee} = \frac{2w\nu_{ee}}{n} \left( \int_0^w dw \sqrt{w} f \right), \quad (17)$$

$$D_{ee} = \frac{4}{3} \frac{w\nu_{ee}}{n} \left( \int_0^w dw w^{3/2} f + w^{3/2} \int_w^\infty dw f \right), \quad (18)$$

$$\nu_{ee} = \frac{4\pi\Lambda_{ee}n}{m^2\nu^3}, \quad (19)$$

where  $w = mv^2/2$  is the electron kinetic energy,  $\nu_{ee}$  is the Coulomb collision frequency, and  $\Lambda_{ee}$  is the Coulomb logarithm.

The energy diffusion coefficient responsible for the electron heating is given by

$$D_\varepsilon(\varepsilon) = \frac{\pi e^2}{4m^2} \sum_{n=-\infty}^{\infty} \int_0^\varepsilon d\varepsilon_x \quad (20)$$

$$\times |E_{yn}(\varepsilon_x)|^2 \frac{\varepsilon - \varepsilon_x}{\Omega_b(\varepsilon_x)} \frac{\nu}{[\Omega_b(\varepsilon_x)n - \omega]^2 + \nu^2}.$$

Note that this expression for  $D_\varepsilon(\varepsilon)$  accounts for the bounce resonance  $\Omega_b(\varepsilon_x)n = \omega$ . The dependance of electron plasma heating on resonant electrons especially pronounced for the  $\nu \ll \omega$ , as in this case

$$\frac{\nu}{[\Omega_b(\varepsilon_x)n - \omega]^2 + \nu^2} \rightarrow \pi \delta(\Omega_b n - \omega) \quad (21)$$

where  $\delta()$  is a Dirac delta function. It is worth to note that if  $L \rightarrow \infty$ , the summation in (21) goes into integration over corresponding wave vectors  $k_n$ , and the bounce resonance condition  $\Omega_b(\varepsilon_x)n = \omega$  transforms into the well-known wave-particle resonance condition for continuous wave spectrum  $kv = \omega$ .

### Calculation of the rf electric field

The transverse rf electric field  $E_y$  is obtained from a single scalar equation

$$\frac{d^2 E_y}{dx^2} + \frac{\omega^2}{c^2} E_y = -\frac{4\pi i \omega}{c^2} [j(x) + I\delta(x) - I\delta(x-L)], \quad (22)$$

where  $I$  is the wall current and  $j(x)$  is the induced electron plasma current density that can be calculated knowing the anisotropic part  $f_{1s}$  of the EVDF

$$j = -\frac{em^{3/2}}{4\pi\sqrt{2}} \int f_{1s} v_y d^3\mathbf{v}. \quad (23)$$

Note that the normalization factor in Eq.(23) appears due to the normalization of  $f_0$  as

$$n_e(x) = \int_{\varphi(x)}^\infty f_0(\varepsilon) \sqrt{\varepsilon - \varphi(x)} d\varepsilon. \quad (24)$$

We now use the Fourier series

$$E_y(x) = \sum_{s=0}^{\infty} \Xi_s \cos(k_s x), \quad (25)$$

where  $s$  is an integer,  $k_s = (2s+1)\pi/L$ . Substituting Eq. (25) into Eq. (22) yields

$$\left( -k_s^2 + \frac{\omega^2}{c^2} \right) \Xi_s = -\frac{4\pi i \omega}{c^2} \left[ j_s + \frac{2I}{L} \right], \quad (26)$$

$$j_s = \frac{e^2}{m} \frac{n_e}{i(2s+1)\Omega_{bT}} \sum_{l=0}^{\infty} \Xi_l Z_{s,l}^{\text{gen}} \left( \frac{\omega + i\nu}{(2s+1)\Omega_{bT}} \right), \quad (27)$$

where  $n_e$  is the plasma density at the discharge center,  $\Omega_{bT} = V_T \pi/L$ ,  $V_T = \sqrt{2T/m}$ , and we introduced the generalized plasma dielectric function [15]

$$Z_{s,l}^{\text{gen}}(\xi) \equiv \sqrt{\frac{2}{m}} \frac{(2s+1)\pi\Omega_{bT}}{n_e L} \sum_{n=-\infty}^{\infty} \int_0^\infty \quad (28)$$

$$\times \frac{\Gamma(\varepsilon)}{n\Omega_b(\varepsilon) - (2s+1)\Omega_{bT}\xi} \frac{G_{s,n}(\varepsilon)G_{l,n}(\varepsilon)}{\Omega_b(\varepsilon)} d\varepsilon,$$

where

$$\Gamma(\varepsilon) = \int_\varepsilon^\infty f_0(\varepsilon) d\varepsilon. \quad (29)$$

In the limit of a uniform plasma, the generalized dielectric function coincides with the standard plasma dielectric function [15]. The coefficients  $G_{l,n}(\varepsilon)$  are the temporal Fourier transforms of  $\cos(k_l x)$  in the bounce motion of an electron in the potential well ( $md^2x/dt^2 = e\phi/dx$ )

$$G_{l,n}(\varepsilon) = \frac{1}{T} \left[ \int_0^T \cos[k_l x(\tau)] \cos\left(\frac{\pi n \tau}{T}\right) d\tau \right]. \quad (30)$$

The Maxwell equation (26) together with the equation for the electron current (27) and (30) comprise the complete system for determining the profiles of the rf electric field.

### Calculation of the electrostatic potential

The electrostatic potential is obtained using the quasineutrality condition

$$n_e(x) = n_i(x) = \int_{\varphi(x)}^\infty f_0(\varepsilon) \sqrt{\varepsilon - \varphi(x)} d\varepsilon, \quad (31)$$

where  $n_e(x)$  is the electron density profile and  $n_i(x)$  is the ion density profile given by a set of fluid conservation equations for ion density and ion momentum [22]

$$\frac{\partial n_i}{\partial t} + \frac{\partial(n_i u_i)}{\partial x} = R, \quad (32)$$

and

$$\frac{\partial(n_i u_i)}{\partial t} + \frac{\partial(n_i u_i u_i)}{\partial x} = -\frac{n_i}{M_i} \frac{\partial \phi(x)}{\partial x} - \nu_i n_i u_i, \quad (33)$$

where  $R$  is the ionization rate,  $\nu_i$  is the ion-neutral collision frequency and  $n_i$ ,  $u_i$ , and  $M_i$  are ion density, velocity, and mass, respectively.

Eq. (31) is solved in the form of a differential equation [20]

$$\frac{d\varphi}{dx} = -T_e^{\text{scr}}(x) \frac{d \ln[n_i(x)]}{dx}, \quad (34)$$

where  $T_e^{\text{scr}}(x)$  is the electron screening temperature

$$T_e^{\text{scr}}(x) = \left[ \frac{1}{2n(x)} \int_{\varphi(x)}^{\infty} f_0(\varepsilon) \frac{d\varepsilon}{\sqrt{\varepsilon - \varphi(x)}} \right]^{-1}, \quad (35)$$

and the electrostatic ambipolar potential can be obtained by integration of Eq.(34).

The above described self-consistent system of equations was formulated in [15], and implemented and compared with the experimental data in [22, 23]. Although the simulation results of the latter articles were proven to be adequate, the method of the direct computation of Green functions, used there, seems to be impractical, because of the excessively long computational time (about a day). To speed up the calculations (to about an hour), the Fast Fourier Transform [Eqs.(26)-(30)] was used in the present simulations.

## RESULTS AND DISCUSSION

Collisionless heating is a very important channel of power transfer for bounded, warm, low-collisional plasmas [4]. For a semi-infinite plasma, the collisionless heating essentially depends on the resonant electrons, i.e. electrons moving with the velocities equal to phase velocities of the components of the spectrum of the driving rf field. Such electrons can effectively gain energy from a wave and, henceforth, the plasma can be efficiently heated under resonant conditions. For the case of bounded plasma, the condition for resonance heating transforms into the bounce resonance condition, i.e., the frequency  $\omega$  of the electromagnetic wave must coincide, or to be several times larger of the bounce frequency  $\Omega_b$  of the electron bounce motion in the potential well. If the electron mean free path is larger than the discharge gap

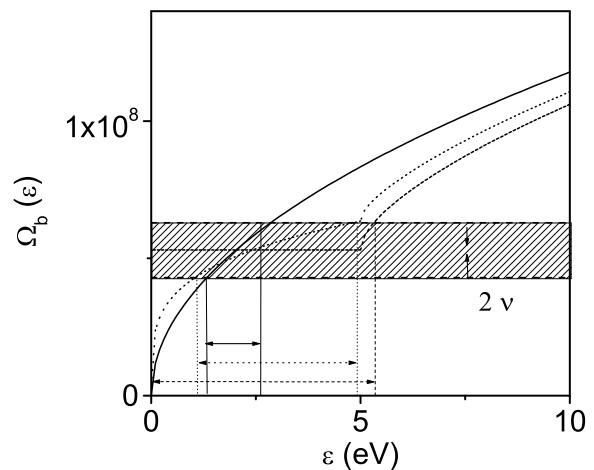


FIG. 1: The electron bounce frequency  $\Omega_b(\varepsilon_x) = \pi/T_b(\varepsilon_x)$ , for discharge of length  $L = 5$  cm, as a function of the electron energy [ $\varepsilon_x = mv_x^2/2 - e\phi(x)$ ] for different potential wells, consisting of the reflecting walls and different ambipolar potentials  $\phi(x)$ . Solid line corresponds to a uniform plasma with  $\phi(x) = 0$ ; dashed line – quadratic potential  $\phi(x) = 5 \times (2x/L - 1)^2$  eV; and dotted line – quartic potential  $\phi(x) = 5 \times (2x/L - 1)^4$  eV. Here,  $T_b(\varepsilon_x) = \int_{x_-}^{x_+} dx/v_x$ ,  $\varepsilon_x(\varepsilon_x)$ . The cross-hatched box shows the resonance region. Arrows show electron energies in the resonance region.

$L$ , the resonant electrons with  $\Omega_b = \omega$  accumulate velocity changes in successive interactions with the rf electric field, which lead to very effective electron heating [5].

The importance of the resonant electrons for plasma heating under the bounce resonance condition, can be readily examined from expression (21) for the electron energy diffusion coefficient, where the term  $\Omega_b(\varepsilon_x)n = \omega$  in the denominator clearly shows the dominant role of the resonant electrons for collisionless electron heating. The total power  $P$  deposited into plasma, per unit square of a side surface, is related to the electron energy diffusion coefficient  $D_\varepsilon(\varepsilon)$  [15],

$$P = -\sqrt{2m} \int_0^\infty D_\varepsilon(\varepsilon) \frac{df_0(\varepsilon)}{d\varepsilon} d\varepsilon. \quad (36)$$

The presence of an ambipolar electrostatic potential can greatly affect the electron heating due to two reasons:

- 1) the ambipolar potential confines low energy electrons to the center of the discharge plasma and these electrons cannot reach the region of the strong field near the walls, and
- 2) the number of resonant electrons is generally larger for a nonuniform plasma than for a uniform plasma due to influence of the electrostatic ambipolar potential on the bounce frequency.

If the ambipolar potential is accounted for, then for low energy electrons, the distance between turning points is smaller than the distance between walls  $L$ . This results to an increase of their bounce frequencies compared to

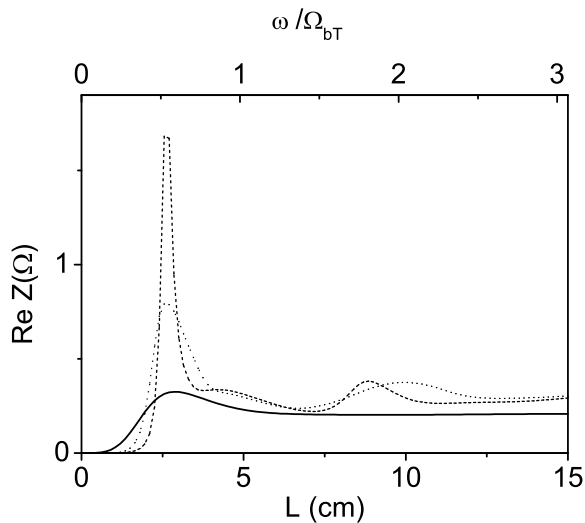


FIG. 2: The plasma resistivity as a function of the distance between the walls for a uniform plasma (without any ambipolar potential) and a nonuniform plasma with the quadratic and quartic potentials and a given Maxwellian EEDF. Discharge parameters are: electron temperature  $T_e = 5$  eV, peak electron density at the center of the discharge  $n_e = 5 \times 10^{11} \text{ cm}^{-3}$ , rf field frequency  $\omega/2\pi = 13.56$  MHz, and electron transport frequency  $\nu = 10^7 \text{ s}^{-1}$ . The lines correspond to the same cases as in Fig. 1.

the uniform plasma case. Therefore, if electrons with low energy were far from the bounce resonance in a uniform plasma, they can approach the resonance region in nonuniform plasma. Fig. 1 shows the dependence of the electron bounce frequency  $\Omega_b(\varepsilon_x)$  on the electron energy  $\varepsilon$  for different potential wells, consisting of the reflecting walls and different ambipolar potentials  $\phi(x)$ . Here,  $\Omega_b(\varepsilon_x) = 2\pi/T_b(\varepsilon_x)$ , where  $T_b$  is half of the bounce period of the electron motion in the potential well  $\varphi(x)$  given by Eq. (6). The width of the resonance is given by Eq.(21) and is proportional to  $\nu$ . The population of resonant electrons consists of all electrons corresponding to the interval of bounce frequencies  $\Omega_b(\varepsilon_x)n \in [\omega - \nu, \omega + \nu]$  where for most practical cases  $n = 1$  – only the first resonance is important. From Fig. 1 it is apparent that the number of resonance electrons increases if the ambipolar potential is accounted for. For example, all electrons confined in the quadratic potential have the same bounce frequency and are all resonant, if the bounce frequency is equal to the discharge frequency. The results of the calculations described below show that increase of the number of the resonant electrons has a much more profound effect on the discharge plasma heating than the mere confinement of them in the region of low rf field.

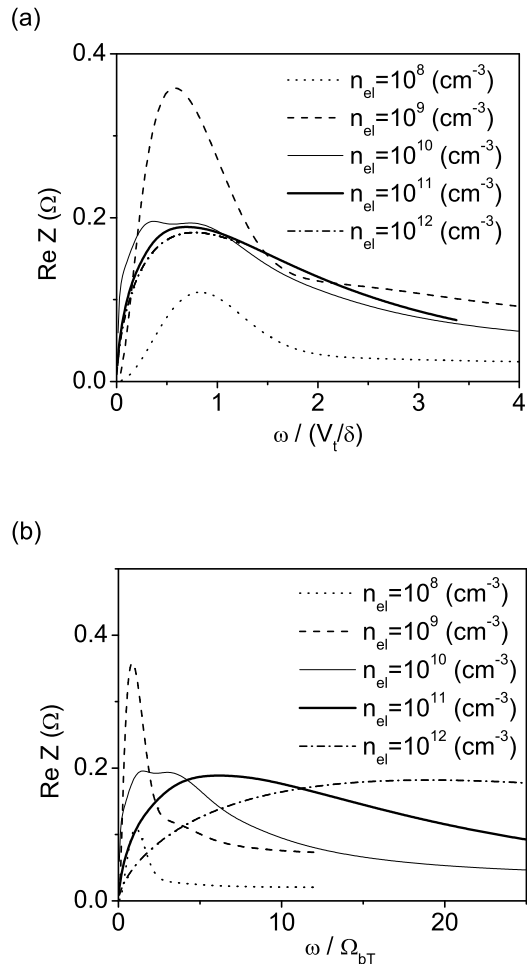


FIG. 3: The plasma resistivity as a function of the driving frequency normalized by (a) the inverse of the transit time through the skin layer  $V_T/\delta_{\max}$  and (b) by the bounce frequency  $V_T\pi/L$ , for different electron densities and for the fixed discharge parameters:  $L = 50$  cm,  $T_e = 5$  eV and  $\nu = 10^6 \text{ s}^{-1}$ . Here,  $V_T$  is the thermal velocity and  $\delta_{\max}$  is the rf field plasma penetration depth for the maximal value of the resistivity at a given density.

#### Non-self-consistent simulations with a given Maxwellian EEDF and given ambipolar potentials

Most of earlier works on low-pressure ICP discharges were reported assuming a Maxwellian EEDF, uniform plasma and accounted for the sheath electric field by bouncing electrons off the discharge walls [8, 10, 11, 12].

In order to explicitly show the importance of accounting for ambipolar potential on collisionless electron heating, we performed numerical simulations using a given Maxwellian EEDF for uniform and nonuniform plasmas (*with* and *without* an ambipolar potential). Specifically, we obtained results for the dependence on the plasma length of the plasma resistivity or the real part

of impedance  $Z = 4\pi/c \times E(0)/B(0)$ , where  $E(0)$  and  $B(0)$  are the electric and magnetic field at the wall, respectively [3]. The surface impedance is related to the power deposition according to:

$$P = -I^2 \text{Re}Z, \quad (37)$$

where  $I$  is the amplitude of the current.

The results are presented in Fig. 2. It is clearly seen that the presence of the ambipolar potential enhances significantly the resistivity of the plasma under the bounce resonance condition, compared to the case of the absence of a potential. The most profound change in resistivity is observed for the quadratic potential. In this latter case all trapped electrons have the same bounce frequency, and thus all of them can be resonant. The obtained results explicitly show that neglecting the ambipolar potential, as is often done for simplicity, can lead to large discrepancies (more than 100 percent), especially for conditions close to the bounce resonance. For large gaps  $L \gg 2\pi\delta = 5$  cm (where the skin depth is  $\delta = 0.79$  cm for the conditions in Fig. 2), the two skin layers near both walls are independent of each other, as the gap width is much larger than the nonlocality length  $l = V_T/\omega = 1.55$  cm. As a result, for  $L > 5$  cm the surface impedance does not depend on the gap width. In the opposite limit  $L \ll 2\delta$ , the electric field profile is linear  $E_y = E_y(0)(1 - 2x/L)$  and the plasma resistivity is mostly determined by the first bounce resonance  $\omega = \Omega_b$ . For uniform plasmas, only slow electrons contribute to the collisionless heating, because the resonant velocity corresponds to  $v_x = \omega L/\pi = V_T L/\pi l \ll V_T$ . If  $L \ll 2\delta$  the number of resonant electrons and the total number of electrons in plasma are decreasing for smaller  $L$ , which leads to a smaller heating. For nonuniform plasmas, the bounce resonance condition  $\omega = \Omega_b$  can not be satisfied for any electron energy for small  $L < 2$  cm and collisionless heating vanishes, see Fig. 2.

The maximum of plasma resistivity occurs at  $L \sim 2\delta$ . Similarly to the case of short gaps, the real part of the surface impedance is mostly due to the first bounce resonance  $\omega = \Omega_b$ , and only slow electrons contribute to collisionless heating for uniform plasma, as  $v_x \sim 2\delta\omega/\pi = V_T 2\delta/\pi l < V_T$ . For nonuniform plasmas, the bounce frequency is higher than in uniform plasmas and most of electrons are in resonance. As a result the surface resonance plotted as a function of the gap width has a pronounced peak compared to the shallow maximum in uniform plasmas, see Fig. 2.

To compare the condition of the bounce resonance  $\omega = \Omega_b$  with the corresponding condition of the transit resonance  $\omega = V_T k$ , additional simulations of the dependence of the plasma resistivity  $\text{Re}Z$  on the driving frequency  $\omega$  were performed for the fixed length  $L = 50$  cm with given Maxwellian EEDF corresponding to the electron temperature  $T_e = 5$  eV, and various electron densities for a uniform plasma (without ac-

counting for the electrostatic potential). In Fig. 3(a) the resistivity is shown as a function of the discharge frequency normalized by the inverse of the “transit” time of the electron pass through the skin layer  $V_T/\delta_{\text{max}}$ , where  $\delta_{\text{max}}$  is the plasma penetration depth of the rf field for the maximal value of the resistivity defined as  $\delta = \int_0^{L/2} dx |E_y(x)/E_y(0)|$ . In Figure 3(b) the plasma resistivity is plotted versus the driving frequency normalized by the thermal bounce frequency  $\Omega_{bT} = V_T\pi/L$ . At high plasma densities ( $> 10^{10} \text{cm}^{-3}$ ) the field penetration depth is much smaller than the discharge gap  $L$  and the effects of the finite discharge gap are unimportant: the maximum of the surface impedance and, correspondingly, the most efficient collisionless electron heating occurs at the “transit” resonance  $\omega \simeq V_T/\delta$ , as for the case of semi-infinite plasmas. At low electron densities (and frequencies) ( $n_e < 10^{10} \text{cm}^{-3}$ ) the electric field penetration depth is of the order of the discharge dimension  $\delta \sim L$ , and as a result the maximum of the surface impedance corresponds to the condition of the bounce resonance  $\omega \simeq \pi V_T/L$ . Note that the absolute maximum of the power dissipation occurs when both conditions for the bounce and transit resonances are met, which occurs for  $L = \pi\delta$  [15]. This happens at  $n_e \leq 10^9 \text{cm}^{-3}$  for the conditions of Fig. 3. At high frequencies  $\omega \gg \pi V_T/\delta$ , the number of resonant electrons is exponentially small and collisionless heating vanishes. The resulting heating depends on the collision frequency and nonlocal effects, as described in Ref. [5].

Accounting for the ambipolar potential enhances considerably the plasma resistivity for the aforementioned case. As shown in Fig. 4, the pronounced maxima of  $\text{Re}Z$  appear for the frequencies that correspond to integer multiples of the bounce frequency  $\omega = n\Omega_{bT}$ , because accounting for the electrostatic potential yields a larger number of the resonant electrons.

### Self-consistent calculations

To investigate the behavior of discharge parameters under the condition of a bounce resonance, the full self-consistent simulations of the EEDF, rf electric field, and ambipolar potential for fixed surface current have been performed for 13.56 MHz rf driving frequency. Figure 5 shows the dependence of the resistivity of the discharge plasma on the discharge dimension. The calculations have been performed for discharge gaps from 3 cm to 10 cm (the discharge can not be sustained for gaps smaller than 3 cm at a given pressure of 3 mTorr). It can be clearly seen that the resistivity of the plasma sharply increases for the discharge gap corresponding to the bounce resonance (about 3 cm). The self-consistent electrostatic potential and ion-electron density profiles are plotted in Fig. 6(a) for two different discharge lengths - 3 cm, corresponding to the bounce resonance condition,

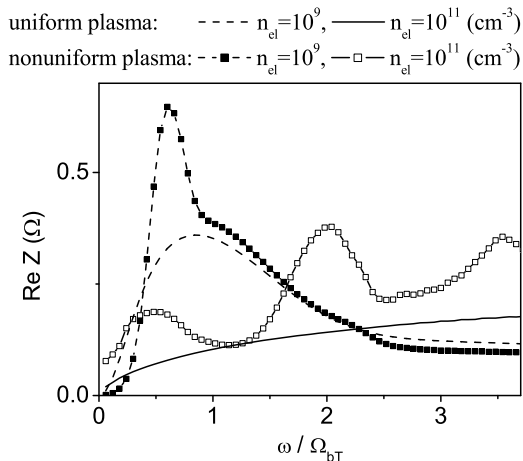


FIG. 4: The plasma resistivity as a function of the driving frequency normalized by the thermal bounce frequency for different electron densities *with* and *without* the ambipolar potential  $\phi(x) = 5 \times (2x/L - 1)^4$  eV and for the same discharge parameters as in Fig.3.

and 10 cm, corresponding to the non-resonant width. These graphs show that the electron density at the center of the discharge is larger for the 3 cm resonant gap than for the 10 cm non-resonant gap. Note that if the power transfer efficiency, or the surface impedance, were the same, then the total power transferred into the plasma would also be the same and the plasma densities would be equal, due to energy balance. In our case the surface impedance for 3 cm gap is considerably higher, what corresponds to the higher plasma density.

The electron energy distribution function and the diffusion coefficient in energy space are shown in Fig. 6(b). Figure 6(b) shows that the energy diffusion coefficient is larger for the 3 cm gap than for the 10 cm gap for electron energy less than 15 eV. This results in more effective electron heating, leading to the larger plasma resistivity shown in Fig. 5. The steady-state electron energy distribution function is governed by the following processes: the collisionless electron heating in the rf electric field, inelastic collisions with neutrals, and re-distribution of energy among plasma electrons due to electron-electron collisions. We see in Fig. 6(b) that the EEDF shape is similar to the two-temperature EEDF [4] with the temperature of the tail of the distribution being lower than the temperature of the main body of the EEDF, corresponding to the onset of inelastic collisional losses. For a 3 cm gap, corresponding to the bounce resonance condition, the electron temperature of low-energy electrons (less than the excitation potential 11.5 eV) is much higher than for the 10 cm non-resonant gap. This effect is similar to the plateau formation on the EEDF governed by collisionless heating in the finite

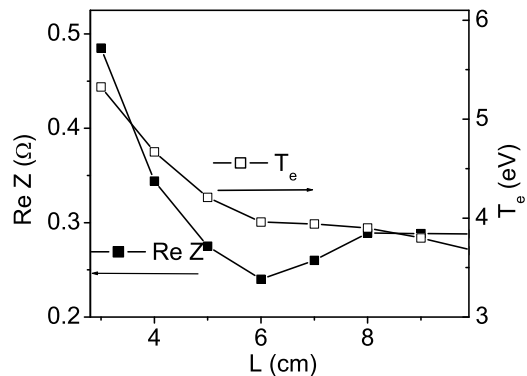


FIG. 5: The results of self-consistent simulations for the plasma resistivity and the electron temperature (defined as  $2/3$  of the average electron energy) at the center of the discharge as functions of the size of the discharge gap and for a given surface current  $I = 5$  A/m, rf field frequency  $\omega/2\pi = 13.56$  MHz and argon pressure  $P = 3$  mTorr.

range of electron energies [6]. Under the conditions of Fig. 6 this plateau is not well pronounced, because it is smeared out by electron-electron collisions. Additional simulations have been performed also for the discharge frequency 6.78 MHz, which is half the driving rf field frequency considered above. For the lower driving frequency the first bounce resonance shifts in the region of larger  $L$ , as shown in Fig. 7. Figure 7 shows the calculated resistivity for two different surface currents, 1 A/cm and 5 A/cm. One can see that the positions of the resistivity maxima corresponding to different surface currents are shifted relatively to each other. The larger surface current corresponds to a larger power transfer into the plasma according to Eq.(37) and results in a higher plasma density ( $n \sim I^2$ ,  $n_e = 2 \times 10^{10}$  and  $n_e = 7 \times 10^{11}$ , respectively). The higher discharge plasma density, in turn, leads to a smaller skin depth. Correspondingly, the position of resistivity maximum shifts into the region of smaller discharge gaps of the order of the skin depth. The electron energy distribution functions for 6.78 MHz are plotted in Fig. 8 for the surface current 1 A/m and for two different lengths, resonant 9 cm and non-resonant 15 cm. The phenomenon of plateau-formation on the EEDF is clearly seen for the bounce resonance condition for  $L = 9$  cm.

## CONCLUSION

The analysis of the properties of inductively coupled discharges clearly shows the phenomenon of the bounce resonance. Self-consistent simulations of the discharge resistivity and electron energy distribution functions demonstrate the significance of the explicit account-

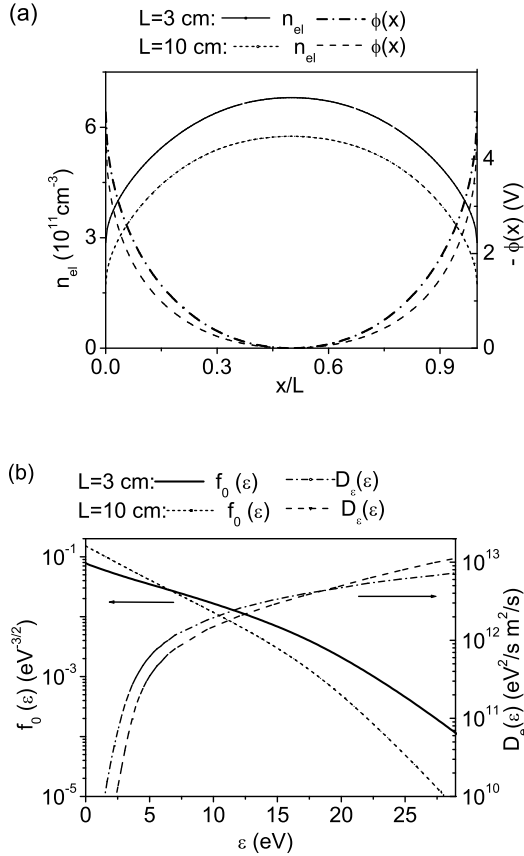


FIG. 6: The results of self-consistent simulations for the discharge gap  $L = 3 \text{ cm}$  corresponding to the bounce resonance, and  $L = 10 \text{ cm}$  for the same conditions as in Fig.5 (a) the electron density and ambipolar potential profiles, (b) the electron energy distribution function EEDF and the energy diffusion coefficient  $D_\epsilon(\epsilon)$  profiles.

ing for the non-uniform plasma density profile and the correct form of the ambipolar electrostatic potential. Enhanced electron heating and larger plasma densities (for a given current in the coil) can be achieved if the low-pressure ICP discharges are operated under the conditions of the bounce resonance.

- 
- [1] M. A. Lieberman and A. J. Lichtenberg, *Principles of Plasma Discharges and Materials Processing*, John Wiley & Sons Inc. (New York) 1994.
  - [2] Francis F. Chen and Jane P. Chang, *Lecture notes on principles of plasma processing*, Kluwer Academic/Plenum Publishers, (New York)(2003).
  - [3] V. I. Kolobov and D. J. Economou, *Plasma Sources Sci. Technol.* **6**, 1 (1997).
  - [4] M. A. Lieberman and V.A. Godyak, *IEEE Trans. Plasma Sci.* **26**, 955 (1998).

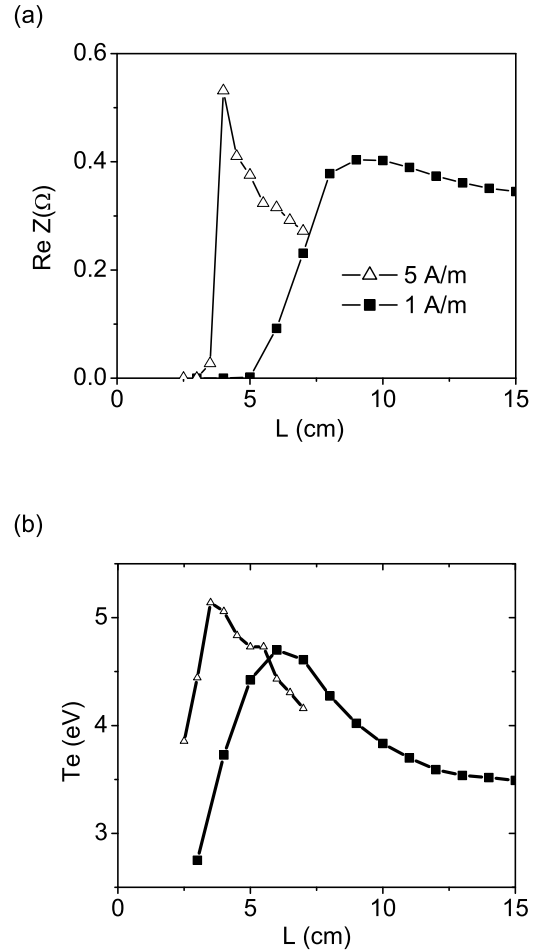


FIG. 7: The self-consistent simulations for two different surface currents  $I = 1 \text{ A/cm}$  and  $I = 5 \text{ A/cm}$  and the given discharge parameters:  $P = 3 \text{ mTorr}$ ,  $\omega/2\pi = 6.78 \text{ MHz}$ . Shown are (a) the plasma resistivity and (b) the electron temperature at the discharge center (two thirds of average electron energy) as functions of the discharge gap.

- [5] I. D. Kaganovich, V. I. Kolobov and L. D. Tsendin, *Appl. Phys. Lett.* **69**, 3818 (1996).
- [6] Yu. M. Aliev, I. D. Kaganovich and H. Schluter, *Phys. Plasmas*, **4**, 2413 (1997); and in more detail, Yu. M. Aliev, I. D. Kaganovich and H. Schluter, "Collisionless electron heating in RF gas discharges. I. Quasilinear theory" in U. Korsthagen and L. Tsendin (Eds.), *Electron kinetics and Applications of glow discharges*, NATO ASI Series B, Physics **367** (Plenum Press, New York and London)(1998).
- [7] U. Buddemeier, I. Kaganovich, "Collisionless electron heating in RF gas discharges. II. Role of collisions and non-linear effects" in U. Korsthagen and L. Tsendin (Eds.), *Electron kinetics and Applications of glow discharges*, NATO ASI Series B, Physics **367**, Plenum Press, (New York and London) (1998).
- [8] K. C. Shaing and A. Y. Aydemir, *Phys. Plasmas* **4**, 3163 (1997).



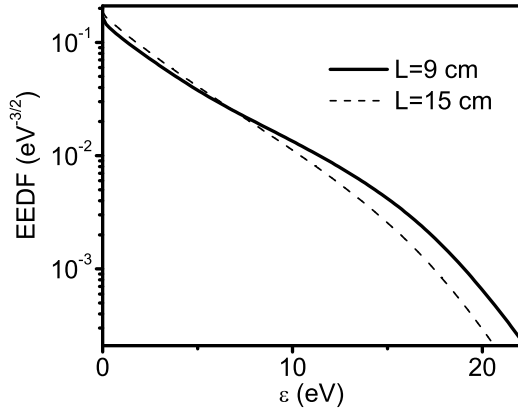


FIG. 8: The electron energy distribution functions for the bounce resonance discharge gap length,  $L = 9$  cm, and for a nonresonant discharge gap  $L = 15$  cm, for the surface current  $I = 1$  A/cm; the other conditions are the same as in Fig. 7.

- [9] I. D. Kaganovich, Phys. Rev. Lett. **82**, 327 (1999).  
 [10] Chin Wook Chung, S. S. Kim, S. H. Seo and H. Y. Chang, J. Appl. Phys. **88**, 1181 (2000).

- [11] Chin Wook Chung, K.-I. You, S. H. Seo, S. S. Kim, and H. Y. Chang, Phys. Plasmas **8**, 2992 (2001).  
 [12] V. A. Godyak and V. I. Kolobov, Phys. Rev. Lett. **81**, 369 (1998).  
 [13] Yu. O. Tyshetskiy, A. I. Smolyakov, and V. A. Godyak, Phys. Rev. Lett. **90**, 255002 (2003).  
 [14] B. P. Cluggish, J. R. Danielson, and C. F. Driscoll, Phys. Rev. Lett. **81**, 353 (1998).  
 [15] I. D. Kaganovich and O. V. Polomarov, Phys. Rev. E **68**, 026411 (2003).  
 [16] B. E. Meierovich, Sov. Phys. JETP **31**, 149 (1971); *ibid.* **10**, 782 (1971).  
 [17] L. D. Tsendin and Yu. B. Golubovskii, Sov. Phys. Tech. Phys. **22**, 1066 (1977).  
 [18] I. D. Kaganovich and L. D. Tsendin, IEEE Trans. Plasma Sci **20**, 66 (1992).  
 [19] I. D. Kaganovich and L. D. Tsendin, IEEE Trans. Plasma Sci **20**, 86 (1992).  
 [20] S. V. Berezhnoi, I. D. Kaganovich and L. D. Tsendin, Plasma Sources Sci. Technol., **7**, 268 (1998).  
 [21] V. L. Ginzburg and A.V. Gurevich, Sov. Phys. Usp. **3**, 115 (1960).  
 [22] B. Ramamurthi, D. J. Economou, and I. D. Kaganovich, Plasma Sources Sci. Technol. **11**, 170 (2002).  
 [23] B. Ramamurthi, D. J. Economou, and I. D. Kaganovich, Plasma Sources Sci. Technol. **12**, 302 (2002);